BAMS Article

Hunting for Gamma Rays above Thunderstorms: The ALOFT Campaign

Timothy J. Lang,[a] Nikolai Østgaard,[b] Martino Marisaldi,[b] Mason G. Quick,[a] Christopher J. Schultz,[a] Ian Adams,[c] Corey G. Amiot,[d] Phillip Bitzer,[e] Richard J. Blakeslee,[a] Robert G. Brown,[f] Kelly Carmer,[e] Hugh Christian,[e] Austin Clark,[e] Morris Cohen,[g] Steven Cummer,[h] Martin Füllekrug,[i] J. Eric Grove,[j] Sebastian Harkema,[e] Gerald Heymsfield,[c] Paul Krehbiel,[k] Rachael Kroodsma,[c] Randall Longenbaugh,[l] Douglas Mach,[m] Matthew Walker McLinden,[c] Andrey Mezentsev,[b] Joan Montanyà,[n] Marni Pazos,[o] David Sarria,[b] Daniel Shy,[j] Mark A. Stanley,[k] Ronald Thomas,[k] T. Daniel Walker,[e] and Camilo Younes[p]

KEYWORDS: Tropics; Convective storms/systems; Lightning; Thunderstorms; Atmospheric electricity; Aircraft observations

ABSTRACT: An internationally collaborative airborne campaign in July 2023—led by the University of Bergen (Norway) and NASA, with contributions from many other institutions—discovered that thunderstorms near Florida and Central America produce gamma rays far more frequently than previously thought. The campaign was called Airborne Lightning Observatory for Fly's Eye Geostationary Lightning Mapper (GLM) Simulator (FEGS) and Terrestrial Gamma-ray Flashes (TGFs), which shortens to ALOFT. The campaign employed a unique sampling strategy with NASA's high-altitude ER-2 aircraft, equipped with gamma-ray and lightning sensors, flying near ground-based lightning sensors. Real-time updates from instruments, downlinked to mission scientists on the ground, enabled immediate return to thunderstorm cells found to be producing gamma rays. This maximized the observations of radiation created by strong electric fields in clouds and showed how gamma-ray production may be physically linked to the thunderstorm life cycle. ALOFT also sampled storms entirely within the stereo-viewing region of the GLM instruments on *GOES-16*/*GOES-18* and performed multiple underflights of the International Space Station Lightning Imaging Sensor (ISS LIS), while using an upgraded FEGS instrument that demonstrated the operational value of observing multiple wavelengths (including ultraviolet) with future spaceborne lightning mappers. In addition, a robust complement of airborne active and passive microwave sensors—including X- and W-band Doppler radars, as well as radiometers spanning 10–684 GHz—sampled some of the most intense convection ever overflown by the ER-2. These observations will benefit planned convection-focused NASA spaceborne missions. ALOFT is an exemplar of a high-risk, high-reward field campaign that achieved results far beyond original expectations.

DOI: 10.1175/BAMS-D-24-0060.1
Corresponding author: Timothy Lang, timothy.j.lang@nasa.gov
Manuscript received 20 February 2024, in final form 14 April 2025, accepted 30 April 2025

SIGNIFICANCE STATEMENT: Though it has been known for years that thunderstorms sometimes produce gamma rays, the Airborne Lightning Observatory for Fly's Eye Geostationary Lightning Mapper (GLM) Simulator (FEGS) and Terrestrial Gamma-ray Flashes (TGFs) (ALOFT) campaign discovered that this high-energy radiation is ubiquitous and highly dynamic in tropical thunderstorms. As these thunderstorms intensify, strong electric fields generate gamma-ray glows, and within those glows, powerful TGFs often occur. When the storms weaken, the gamma-ray production weakens. This means gamma rays can be an indicator of thunderstorm evolution, like lightning flash rate. Thus, thunderstorm radiation is not just a boutique topic for lightning physicists, but also relevant to forecasters, storm scientists, and those impacted by aviation hazards. Moreover, ALOFT gathered important validation data for spaceborne lightning sensors and sampled some of the most intense convection ever overflown by NASA aircraft.

AFFILIATIONS: [a] NASA Marshall Space Flight Center, Huntsville, Alabama; [b] University of Bergen, Bergen, Norway; [c] NASA Goddard Space Flight Center, Greenbelt, Maryland; [d] NASA Postdoctoral Program, NASA Marshall Space Flight Center, Huntsville, Alabama; [e] University of Alabama in Huntsville, Huntsville, Alabama; [f] University of Central Florida, Orlando, Florida; [g] Georgia Institute of Technology, Atlanta, Georgia; [h] Duke University, Durham, North Carolina; [i] University of Bath, Bath, United Kingdom; [j] U.S. Naval Research Laboratory, Washington, D.C.; [k] New Mexico Institute of Mining and Technology, Socorro, New Mexico; [l] Sandia National Laboratories, Albuquerque, New Mexico; [m] Universities Space Research Association, Huntsville, Alabama; [n] Universitat Politècnica de Catalunya, Barcelona, Spain; [o] Universidad Nacional Autónoma de México, México City, México; [p] Universidad Nacional de Colombia, Manizales, Colombia

1. Introduction

About 30 years ago, it was discovered that a thunderstorm is the birthplace of the most energetic natural particle acceleration on Earth, and Terrestrial Gamma-ray Flashes (TGFs) are the most explosive manifestation of such a process (Fishman et al. 1994; Dwyer et al. 2012). TGFs can deliver 10^{18} high-energy photons from thunderclouds to space in a few tens of microseconds (e.g., Dwyer and Smith 2005). Lightning and TGFs are closely related, but the details of this relationship are yet to be fully understood (Cummer et al. 2005, 2011; Stanley et al. 2006; Williams et al. 2006; Tran et al. 2015; Belz et al. 2020; Heumesser et al. 2021; Wada et al. 2020; Lyu et al. 2021; Lindanger et al. 2022; Skeie et al. 2022). For example, TGFs are predominantly associated with high-altitude (>10 km MSL) intracloud lightning (e.g., Cummer et al. 2014), yet TGFs have also been observed in conjunction with cloud-to-ground flashes (e.g., Pu et al. 2020). Glows are another hard-radiation phenomenon in thunderstorms (e.g., Parks et al. 1981; Eack and Beasley 2015; Wada et al. 2023). They likely occur due to relativistic runaway electron avalanches (RREAs) and have much lower flux than TGFs but are longer-lived, and thus they may have a larger effect on the local atmosphere (e.g., Kelley et al. 2015; Wada et al. 2019a; Kochkin et al. 2021).

The phenomenology of TGFs and glows has been poorly understood. A major reason for this is a lack of observations. For example, most spaceborne platforms have measured only hundreds to a few thousand TGFs over their multiyear lifetimes (Grefenstette et al. 2009; Briggs et al. 2013; Østgaard et al. 2019b; Maiorana et al. 2020). By contrast, the Geostationary Lightning Mapper (GLM) measures millions of lightning flashes per year (Rudlosky et al.

2019; Rudlosky and Virts 2021). Meanwhile, glows can only be measured via ground- or aircraft-based sensors (e.g., Chilingarian et al. 2011; Kelley et al. 2015; Kochkin et al. 2017; Østgaard et al. 2019a; Wada et al. 2021b; Kuriyama et al. 2022); there is no instrument currently sensitive enough to detect glows from space.

In the literature, there is potentially contradictory information regarding how TGFs are related to thunderstorm evolution. For example, Chronis et al. (2016) found that a variety of storm types can produce TGFs, and TGFs have even been observed in winter thunderstorms (e.g., Wada et al. 2019b). Meanwhile, Ursi et al. (2019) found that TGFs can be associated with the mature phase of thunderstorms, an observation also supported by van der Velde et al. (2024), while other studies (Splitt et al. 2010; Barnes et al. 2015; Tiberia et al. 2021) found that TGF-producing storms tend to appear taller and/or stronger than other thunderstorms. However, Smith et al. (2010) and Larkey et al. (2021) found TGFs tend to occur during times of low or declining flash rates. Another question is why TGFs seem to be more common in oceanic thunderstorms (Lindanger et al. 2020). For that matter, do spaceborne sensors even measure a representative sample of TGFs (Bjørge-Engeland et al. 2024)? For example, the mean free path of gamma rays in the atmosphere can be short (Williams et al. 2022, 2023); could the spaceborne climatology of TGFs be biased because gamma rays associated with high-altitude lightning (e.g., Cummer et al. 2014) in tall tropical thunderstorms have a better chance of escaping to space?

Glows are more common than TGFs and appear to be associated with strong electric fields that accelerate electrons to relativistic speeds, leading to particle collisions and subsequent release of bremsstrahlung gamma and X-rays (Kelley et al. 2015). However, they lack the relativistic feedback mechanism that creates the high-energy TGFs (Dwyer 2012). Since they are related to electric field strength, glows have been more reliably tied to indicators of thunderstorm development, such as radar reflectivity (Wada et al. 2021a; Williams et al. 2022, 2023). But are glows necessarily precursors to TGFs? Is there a competition between TGFs, glows, and regular lightning for electric field energy?

Thus, overall, there has been limited consensus in the thunderstorm gamma-ray community on 1) how and under what meteorological conditions TGFs are produced, and 2) how common glows are and how they relate to TGF production and thunderstorm life cycle. What was needed to address this uncertainty were high-resolution/sensitivity measurements of TGFs, glows, and their related source lightning and thunderstorms. Specifically, these measurements needed to be made using aircraft flying over tropical and subtropical thunderstorms, which are widely recognized as the most common generators of satellite-detected TGFs (e.g., Morales Rodriguez et al. 2021).

Moreover, since the GLM instruments on the GOES-R series of satellites (*GOES-16*, *GOES-17*, *GOES-18*, and *GOES-19*) were launched starting in late 2016, only one dedicated airborne campaign for calibration and validation has occurred, during spring/summer 2017. That campaign, called the GOES-R Post-Launch Test (PLT), only underflew *GOES-16's* GLM (Quick et al. 2020). The current GOES-West (*GOES-18*) GLM had not benefitted from direct optical-to-optical validation from an airborne platform. During the GOES-R PLT, the NASA ER-2 carried the Fly's Eye GLM Simulator (FEGS), a set of radiometers that measures high-resolution optical output from lightning in clouds. At the time, FEGS featured radiometers with the same 777-nm near-infrared (IR) band as GLM but did not carry a radiometer for the 337-nm ultraviolet (UV) band. This UV band provides highly complementary information about lightning processes, especially streamers that are much cooler than hot leader channels, which are optically bright across many spectral bands (da Silva and Pasko 2013; Walker and Christian 2017). Notably, lightning streamers can be physically related to TGFs and can occur in concert with narrow bipolar events (NBEs) that are dim at 777 nm (Soler et al. 2020). Indeed, it is highly likely that a significant population of

lightning is completely missed by GLM, especially those that are dominated by streamers as opposed to leaders, or that are weak and dim overall (Marchand et al. 2019; Murphy and Said 2020; Rutledge et al. 2020; Lang 2023).

Thus, there is increasing interest in coupled 337-/777-nm observations of lightning, especially at the high spatial and temporal resolutions offered by airborne measurements. These observations can support not only UV/IR observations provided by existing spaceborne lightning sensors like the Atmosphere–Space Interaction Monitor (ASIM; Neubert et al. 2019) but also bispectral optical observations from potential future missions like CubeSpark (Remington et al. 2024). It would also be of interest to validate a recently developed algorithm for determining cloud-top heights from stereo GLM (i.e., GOES-East and West) observations using direct measurements from an airborne platform (Mach and Virts 2021).

In addition, the International Space Station Lightning Imaging Sensor (ISS LIS; Blakeslee et al. 2020) was launched in early 2017 and featured the flight-spare LIS instrument that was the low-Earth orbit (LEO) forerunner to GLM, using the same 777-nm band. FEGS was able to underfly ISS LIS only twice during the GOES-R PLT. Since these overpasses last only ~90 s, ISS LIS would benefit from additional underflights for extremely useful optical-to-optical validation comparisons. This was especially urgent since the ISS LIS mission was ending in late 2023. Moreover, ASIM (which launched in 2018) has never benefitted from dedicated airborne underflights.

Finally, there are planned future spaceborne missions, like the Investigation of Convective Updrafts (INCUS; Dolan et al. 2023) and Atmosphere Observing System (2024), whose science will benefit from suborbital measurements, including those made prior to launch—similar to how the Global Precipitation Measurement (GPM) mission benefitted from prelaunch suborbital campaigns (Jensen et al. 2016; Skofronick-Jackson et al. 2015). Major goals of these missions are to measure parameters like vertical air motion, convective mass flux, ice water content, and related quantities in convective clouds using Doppler radars and high-frequency radiometers. It is widely recognized that these observations are highly synergistic with lightning measurements (e.g., Liu and Zipser 2008; Reinhart et al. 2014). These future missions are especially interested in documenting convective processes, so frequent sampling of evolving storms using aircraft is desired.

To meet the above challenges and opportunities, the Airborne Lightning Observatory for FEGS and TGFs (ALOFT) campaign was conceived. ALOFT was a collaboration between the University of Bergen (UIB), NASA, and many other institutions, and it is an excellent example of a highly focused, low-cost field campaign that benefitted from taking significant scientific risks. The objectives for ALOFT were the following:

1) Observe TGFs in one of the most TGF-intense regions on the planet.
2) Observe gamma-ray glows in thunderstorms and their relation to TGFs.
3) Perform ISS LIS and GLM validation using improved suborbital instrumentation.
4) Evaluate new design concepts for next-generation spaceborne lightning mappers, including the value of multispectral observations.
5) Make combined microwave and lightning measurements of convection from a suborbital platform.

2. Campaign design

a. Aircraft and ground instrumentation. ALOFT used the NASA ER-2 as its airborne platform. This aircraft flies at approximately 20-km MSL at a ground speed of ~200 m s^{-1} and has been used in many convection-focused field campaigns, in both the midlatitudes and the tropics (e.g., Halverson et al. 2007; Jensen et al. 2016). The ER-2's high-altitude capability was critical for ALOFT, to be able to overfly often tall (up to ~18 km) tropical thunderstorms.

Table 1. ER-2 instrument payload for ALOFT.

Instrument name	Description	Measurement/reference
UIB-BGO	Scintillator 300 keV–40 MeV, 0.1-/0.5-μs sampling	TGFs, glows (Østgaard et al. 2024)
iSTORM	Scintillator 300 keV–5 MeV, <1-μs sampling	TGFs, glows (Østgaard et al. 2024)
FEGS	25- × 780-nm radiometers 340-, 500-, 870-, 1600-, and 300–1100-nm radiometers (10-μs sampling) HD camera, spectrometer	Optical detection of lightning processes, flash mapping (Quick et al. 2020)
EFCM	Fast (0.1 μs) and slow (1 μs) measurements of electric field change	Flash counting, lightning physical processes (Quick et al. 2020)
LIP	7 × rotating vane electric field mills (20-ms sampling)	3D electric field vectors, lightning (Schultz et al. 2021)
AMPR	10.7, 19.35, 37.1, and 85.5 GHz Dual-polarization, cross-track scanning	Precipitation, cloud liquid water and ice, water vapor, ocean winds (Amiot et al. 2021)
CoSSIR	170, 177.31, 180.31, 182.31, 325 ± 11.5, 325 ± 3.4, 325 ± 0.9, 684 GHz Dual-polarization, conical and along-track scanning	Cloud ice, snow, water vapor (Kroodsma 2024)
EXRAD	X-band conical-scanning and nadir-staring Doppler radar	Precipitation 3D structure, vertical velocity (Heymsfield et al. 2024)
CRS	W-band nadir-staring Doppler radar	Cloud vertical structure, vertical velocity (Walker McLinden et al. 2021)

The airborne payload is shown in Table 1. Two gamma-ray instruments [UIB–Bismuth Germanium Oxide (BGO) and in Situ Thunderstorm Observer for Radiation Mechanisms (iSTORM)], the optical FEGS instrument, plus electric field [Lightning Instrument Package (LIP)] and electric field change meter (EFCM) sensors formed the core scientific payload. Complementing these instruments were X-band Doppler radar (EXRAD) and W-band [Cloud Radar System (CRS)] Doppler radar, along with passive microwave [Advanced Microwave Precipitation Radiometer (AMPR)] to submm [Configurable Scanning Submillimeter-wave Instrument/Radiometer (CoSSIR)] radiometers. These four microwave (broadly speaking) sensors were leveraged from the Investigation of Microphysics and Precipitation for Atlantic Coast-Threatening Snowstorms (IMPACTS; McMurdie et al. 2022) campaign, which had ended a couple of months before ALOFT integrated. Taken together, the overall ALOFT payload would provide an excellent mix of detailed observations of lightning and high-energy physical processes coupled with multifrequency observations of convective structure and evolution.

Ground instruments were strategically located throughout the ALOFT domain (Fig. 1). A list of core sensors is shown in Table 2. The low-frequency (LF) antennas provided long-range detection and were important for documenting physical processes related to lightning and TGFs (Pu et al. 2019). Meanwhile, the Central Florida Lightning Mapping Array (CFLMA), interferometer, and Panama Marx Meter Array (PAMMA) sensors provided 2D/3D flash mapping, albeit over much shorter ranges than the LFs. In addition to the LF and interferometer, the San Andres Island location featured other sensors, such as a very high frequency (VHF) receiver (i.e., single LMA station), a high-speed camera, high-energy detectors, and a C-band radar.

The ER-2 was based at MacDill Air Force Base in Tampa, Florida. With a flight duration that normally reaches 8 h, enabling a maximum range of approximately 2700 km, the ER-2 was able to travel as far south as San Andres Island (part of Colombia), off the eastern coast of Nicaragua, and still provide up to 2 h on-station time. This basing brought most known TGF hotspots near Florida and Central America within useful range, except for mainland Panama, the Bight of Panama, and northwestern Colombia (Fig. 1). Note that in the Americas,

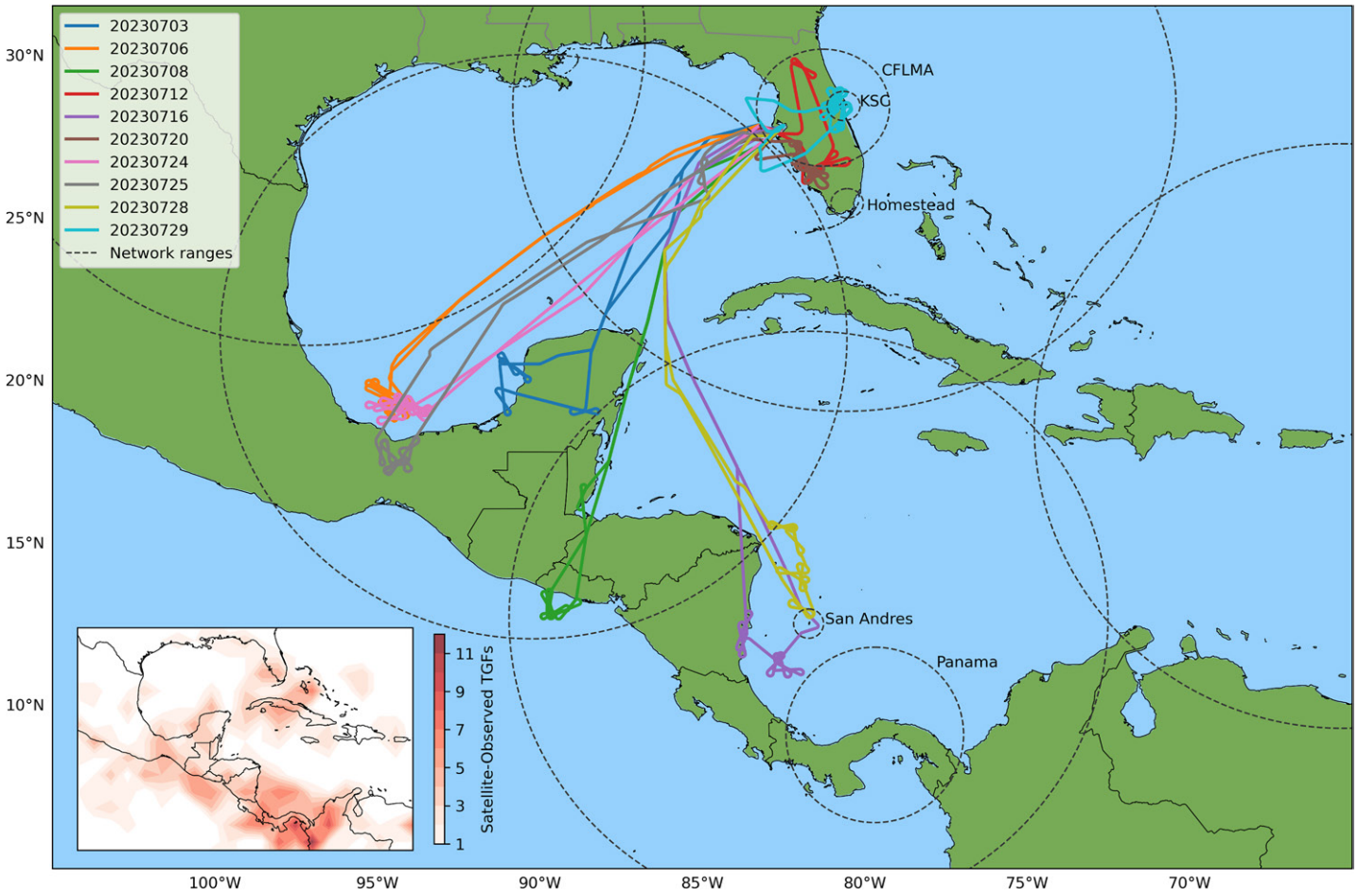

Fig. 1. Map of the ALOFT domain, including flight tracks from the 10 research missions and the nominal ranges of various ground-based lightning networks. The inset shows the domain's satellite-based TGF climatology during June–August from ASIM and the Fermi Gamma-ray Burst Monitor (GBM).

these satellite-detected TGF hotspots are primarily in coastal or offshore regions. The reasons for this are not well understood, though a contributing factor may be the propensity of these regions to generate intense, organized thunderstorms. In particular, there is a well-known diurnal cycle in sea-/land-breeze circulations and associated convection and rainfall, with thunderstorms favored over land during daytime but then transitioning offshore overnight. The Isthmus of Tehuantepec in southern México provides a notable example of such behavior (Curtis 2004).

Unfortunately, only a minority of ALOFT flights were able to take advantage of the short-range flash mapping networks (e.g., CFLMA), though LF support was available for all flights. All ALOFT flights were within the stereo-viewing region of GLM-16/East and GLM-18/West (Mach and Virts 2021; Rudlosky and Virts 2021; Marisaldi et al. 2024; Østgaard et al. 2024).

Table 2. Primary ground-based instruments used in ALOFT. Maximum ranges are approximate. Sensor performance is always better closer to each sensor/network.

Instrument	Range/location(s)	Measurement/reference
CFLMA	200 km (Central Florida)	Lightning 2D/3D mapping (Rison et al. 1999)
LF Antennas	1000 km (Southeast United States; Yucatán, México; San Andres; Puerto Rico)	Lightning physical processes, TGFs (Cohen et al. 2018; Pu et al. 2019)
Broadband VHF Interferometers	75 km (central and southern Florida, San Andres)	High-resolution lightning mapping (Belz et al. 2020; Jensen et al. 2021; Urbani et al. 2021; Pu and Cummer 2024)
PAMMA	300 km (Panama)	3D lightning mapping and electric field changes (Yanoviak et al. 2017; Zhu et al. 2020)

b. "Code glow". Perhaps the most unique part of ALOFT sampling strategy was the need to immediately revisit thunderstorms found to be glowing gamma rays in real time. Gamma-ray-glowing episodes can last only a few minutes or less (e.g., Wada et al. 2019a, 2021a; Kochkin et al. 2021), although they sometimes can last significantly longer (e.g., Williams et al. 2023), but normally it takes 10–15 min for mission scientists to successfully relay updated coordinates to the ER-2 and for the pilot to redirect the aircraft accordingly. Thus, to effectively refly glowing storms, the pilot needed to be empowered to react quickly to news of a glow. As a NASA campaign, ALOFT made use of the Mission Tools Suite (MTS), which enables mission scientists to monitor real-time feeds from a geostationary satellite, ground radar, and ER-2 instruments. UIB-BGO continuously downlinked a 1-s resolution time series of total high-energy particle counts. This is comparable in resolution to many other glow observations in the literature (e.g., Wada et al. 2021a), though it was significantly finer temporal resolution than some approaches (e.g., Williams et al. 2023). Regardless, the 1-s data were sufficient for mission scientists to identify glows (though not TGFs) and immediately relay the alert "code glow" to the pilot in the aircraft via another ground-based "mobile" ER-2 pilot. Prior to the campaign, the pilots were briefed on how to react to a code glow. If the cell in question was easily visible (e.g., daytime, isolated storm), the pilot would immediately execute a bowtie pattern to repeatedly intercept the storm from different approach angles (which speeds up ER-2 turns) until updated coordinates could be delivered by the mission scientists. If the cell was not easily visible (e.g., nighttime, multicellular storm), the pilot was instructed to execute a slower 180° turn that would put the aircraft back toward the storm along the same line and continually refly that line again until updated coordinates were received. The code glow procedure would allow a glowing thunderstorm to be revisited in as quickly as 5–6 min (especially using bowties), enabling process-driven sampling. In practice, during the campaign, the mean revisit time for a bowtie on a specific cell was 8.1 min.

c. Satellite and weather forecast support for ALOFT. The domain for ALOFT was Florida, Central America, and the Caribbean (Fig. 1). This region is covered continuously by both the GOES-East (16) and GOES-West (18) satellites, including the GLMs. The northern portion (e.g., Florida) falls within the 5-min continental United States (CONUS) updates provided by the Advanced Baseline Imager (ABI), but the southern portion (including much of Central America) does not. ALOFT applied for and was granted dedicated mesoscale domain sector (MDS) scans from either *GOES-16* or *GOES-18* ABIs for 7 of its 10 flights. Thankfully, only the three Florida-specific flights (12–13, 20, and 29 July; Fig. 1), which at least had 5-min CONUS coverage, lacked MDS support.

Weather forecasting support was provided by an early career team of three graduate students and one postdoctoral researcher, two of whom had forecasted for previous ER-2 campaigns (including the GOES-R PLT). Apart from the normal consultation of a variety of U.S. and European meteorological forecast models, including terminal aerodrome forecasts (TAFs) for the Tampa area, the team reported on overpass predictions for the ISS (LIS and ASIM, the latter of which can detect TGFs) and the Fermi satellite (which also can detect TGFs; Briggs et al. 2013). These predictions came via the NASA Langley Research Center (LaRC). Regional Weather Research and Forecasting (WRF) Model forecasts from the Caribbean Institute for Meteorology and Hydrology (CIMH) and the Mexican and Salvadoran weather services, as well as the experimental Caribbean High-Resolution Rapid Refresh (HRRR) runs, were also consulted. These mesoscale forecast tools were especially important for the southern portion of the ALOFT domain, which was not covered well by standard U.S. mesoscale models. Go/no-go decisions for flights considered these forecasts as well as the evolving accomplishments relative to the science goals of the campaign.

3. Select initial scientific results

a. On ALOFT scientific risks. Like many NASA airborne campaigns, a mission science scorecard was developed for ALOFT. This scorecard tracked the performance of the campaign against its mission requirements. Chief among these requirements were 1) the detection of at least one gamma-ray glow by the UIB-BGO or iSTORM instruments and 2) the detection of at least one TGF by one of those instruments. Though this sounds like a low bar, prior to ALOFT, the global occurrence of TGFs was thought to be as low as $\sim 10^4$ times less frequent than lightning (e.g., Fuschino et al. 2011; Briggs et al. 2013; Marisaldi et al. 2013; Tierney et al. 2013; Maiorana et al. 2021), though some estimates were higher (e.g., Smith et al. 2011b). Moreover, a couple weak glows were detected during only one flight of the GOES-R PLT in 2017, which was the only previous campaign for the combined FEGS, EFCM, UIB-BGO, iSTORM, and LIP observing suite (Østgaard et al. 2019a). No TGFs were detected during that campaign. Previous airborne campaigns with an instrument called the Airborne Detector for Energetic Lightning Emissions (ADELE) fortuitously detected one TGF in a Florida thunderstorm (Smith et al. 2011a) and one TGF in a hurricane eyewall (Bowers et al. 2018). Thus, while it was possible to observe gamma rays from an aircraft, there was no guarantee that a campaign would detect even one TGF, much less a glow. This made achieving the primary science goals for ALOFT risky—that is, unless TGFs and glows turned out to be nearly ubiquitous in tropical and even subtropical thunderstorms.

b. ALOFT glows and TGFs featuring the 3 July 2023 case. For all results that follow, a glow will be defined as a 1-s total UIB-BGO particle count rate 1.25 times the background (which was determined during a time period right before overflying a particular storm). This is similar to Marisaldi et al. (2024), but additionally in this paper, we will require straight-and-level flight while on station (see Table 3 for times), so that the glows can be best compared to other instruments.

Table 3. Summary statistics for each ALOFT science flight. For ABI and GLM Stereo height biases, positive numbers mean that the satellite-derived height is higher than the CRS CTH. Abbreviations not otherwise defined in the text: Yuc = Yucatán, CB = Campeche Bay, ES = El Salvador, FL = Florida, SA = San Andres, S MX = Southern México, O = Ocean, L = Land, D = Day, and N = Night.

Takeoff date	3 Jul	6 Jul	8 Jul	12 Jul	16 Jul	20 Jul	24 Jul	25 Jul	28 Jul	29 Jul
Location	Yuc	CB	ES	FL	SA	FL	CB	S MX	SA	FL
Ocean/land?	O	O	O	L	O	L	O	L	O	L
Day/night?	D	N	N	D	D	D	N	N	D	D
On station (UTC)	2250–0020	0400–0740	0420–0740	2330–0120	1310–1620	2120–0000	0500–0830	0100–0320 (26 Jul)	1530–1820	1900–2150
Glows	9	35	17	0	6	12	230	19	4	29
TGFs or similar	1	31	5	0	1	2	83	7	1	7
FEGS 340:780 ratio	26%	25%	28%	20%	37%	32%	42%	27%	38%	38%
FEGS flashes (10+ pulses)	111	1395	629	251	288	1695	1991	1380	130	1051
GLM-16 DE	50%	80%	77%	53%	55%	65%	82%	79%	33%	58%
GLM-18 DE	43%	77%	69%	18%	26%	22%	77%	84%	21%	27%
Median CRS CTH (km)	15.6	15.7	14.7	13.0	15.7	15.4	16.6	14.5	15.6	14.7
GLM stereo RMSE (km)	6.3	1.4	2.4	5.5	1.7	1.9	1.3	2.9	1.9	3.9
GLM stereo Bias (km)	−4.3	0.0	−0.6	−4.3	1.0	0.0	0.7	−1.0	1.3	−0.4
ABI RMSE (km)	2.2	3.7	2.2	2.8	1.6	3.0	2.1	4.8	1.1	4.2
ABI Bias (km)	−0.2	1.1	−0.4	0.0	−0.3	0.2	−0.5	2.2	0.2	−0.2

The first science flight was on 3 July, and this sampled convection over and near the Yucatán Peninsula as it was moving offshore (Fig. 1). On the first science leg over the first target storm sampled that first flight, a glow was detected in real time using the UIB-BGO feed (Fig. 2a). The code glow protocol was immediately put into action, and the return leg within ~6 min detected an even stronger glow. Subsequent postflight analysis confirmed a TGF was observed during that second leg (by both UIB-BGO and iSTORM), around 2320:02.945 UTC. Thus, within the first two legs of the first science flight, both minimum requirements for ALOFT were met. Subsequent flights showed this was no accident. Østgaard et al. (2024) and Marisaldi et al. (2024) reported over 130 TGFs or TGF-like events and about 500 glows, respectively, on 9 of the 10 ALOFT flights. This is a level of success that was never anticipated prior to the campaign. Table 3 shows the number of glows and TGFs observed per case. (The more restrictive glow definition in this study resulted in 361 total glows being identified.) Most TGFs or TGF-like events were observed within the presence of a glow.

In fact, glowing thunderclouds became so common and predictable that the code glow procedure eventually became less necessary, as mission scientists learned to target the strongest available cell (via ABI cloud-top temperatures and GLM flash extent density, including trends, as observed in MTS) with preplanned bowties and to simply adjust the center of the pattern as cells moved and evolved. In other words, glows eventually could be anticipated with good skill by targeting cells in their intensifying to mature stages (e.g., using near-real-time geostationary lightning and cloud observations as well as near-real-time airborne electric field, lightning, radar, and radiometer observations in MTS), with the UIB-BGO feed serving as confirmation.

At the time of the TGF on 3 July (Fig. 2e), FEGS detected optical activity, but only in the 340-nm channel (10-nm bandwidth, thus sensitive to 337-nm line emission associated

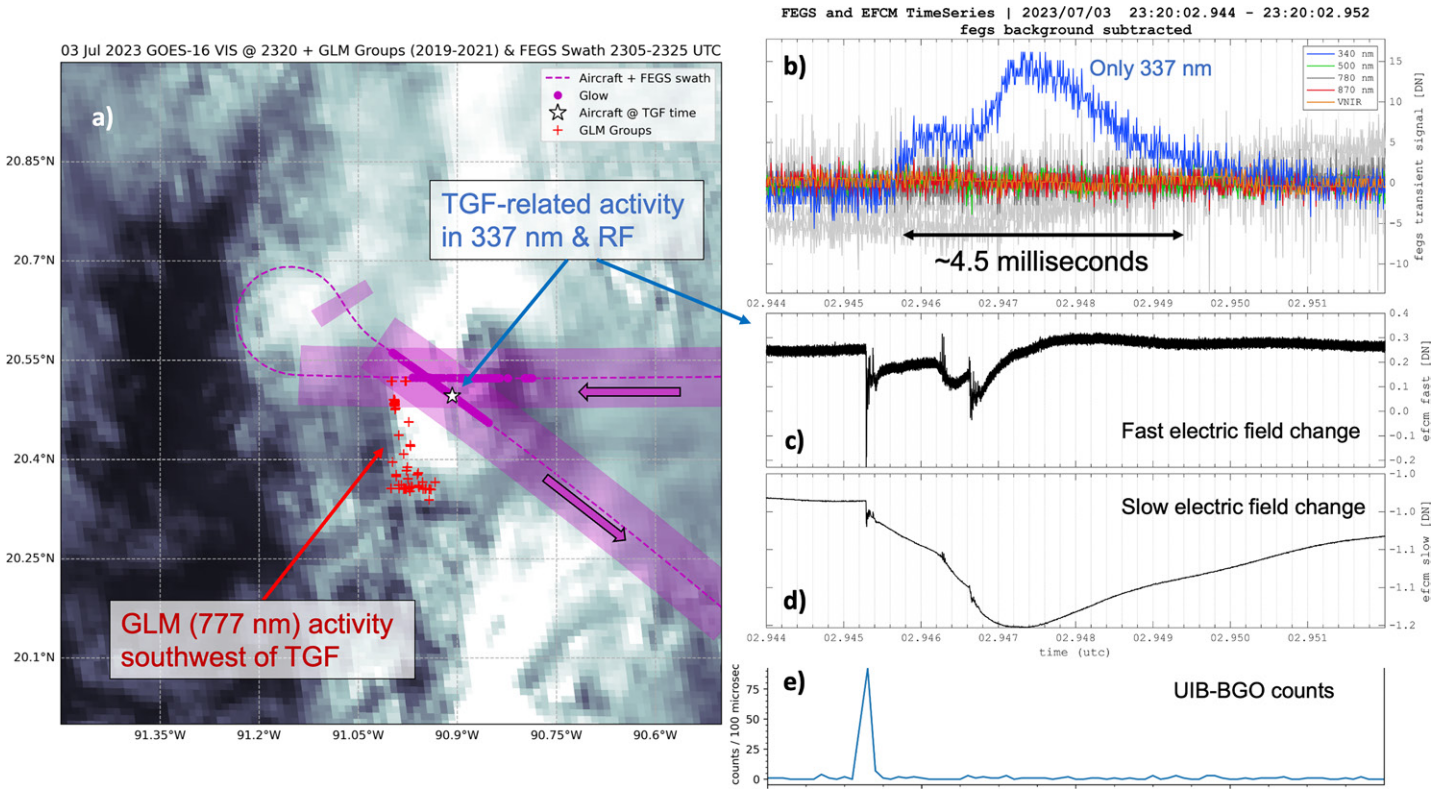

FIG. 2. Overview of the 2305–2325 UTC legs on 3 Jul 2023, off the west coast of the Yucatán Peninsula. (a) *GOES-16* ABI visible channel at 2320 UTC, along with the locations of GLM-16 groups (2019–2100 UTC), and the location of the aircraft when glows and the TGF were detected. The aircraft track, travel direction, and approximate FEGS swath are also indicated. (b) Time series of signals from multiple FEGS channels, showing only response in the 340-nm channel (sensitive to 337-nm line emission) around the time of the TGF (approximately 2320:02.945 UTC). (c) Time series of fast and (d) slow EFCM channel response on the same time scale as (b). (e) UIB-BGO counts per 100 *μs* for the same time period as (b)–(d).

with lightning streamers; Fig. 2b). This pulse lasted for approximately 4.5 ms, and both the fast and slow channels on the EFCM indicated multiple electric field changes during the pulse, which also matched with modulations in the 340-nm pulse signal strength. This is an excellent example of the synergy observing the 337-nm emission line has with more traditional 777-nm observations (sensitive to hot leader channels). The GLM-16 groups were clustered mostly southwest of the aircraft flight track (Fig. 2a); indeed, based on GLM and the FEGS swath, one might expect very little lightning activity in the FEGS field of view during these legs, although parallax could be affecting GLM group locations. Regardless, lightning streamer-only activity is largely invisible at 777 nm, and the complementarity of 337 nm when observing TGFs and other streamer-based pulses has been repeatedly demonstrated using the ASIM mission on the ISS (e.g., Soler et al. 2020). However, ASIM optical detections only occur at night; the 3 July flight occurred over a sunlit cloud (Fig. 2a), confirming the daytime utility of 337-nm observations. During ALOFT, the ratio of FEGS 340-nm pulses to (nadir) 780-nm pulses (10-nm bandwidth) ranged from 20% to 42% (Table 3), and many of the 340-nm pulses were unique, with no 780-nm counterpart like the one shown in Fig. 2b. Interestingly, the most productive TGF and glow case (24 July) was an intense storm system (Marisaldi et al. 2024) that also featured the highest ratio of 340-nm pulses, while the relatively weak nonglow/TGF case on 12 July (discussed in the next section) featured the lowest 340-nm ratio, suggesting the ratio of streamers to leaders may vary significantly depending on thunderstorm characteristics, supporting the results of Husbjerg et al. (2022) regarding the phenomenology of 337-nm discharges observed by ASIM. Work is ongoing to fully analyze 340- versus 780-nm pulses in ALOFT, but early results suggest that observing in the UV in addition to near-IR would provide a more comprehensive assessment of lightning production by a thunderstorm.

c. Validation of spaceborne lightning observations featuring the 12–13 July 2023 case. The science flight on 12–13 July targeted an ISS overpass. While other ISS underflights occurred on 20 (aircraft in turn), 24 (LIS temporary malfunction, although ASIM was operating; Bjørge-Engeland et al. 2024), 25–26 (no lightning due to decaying storm), and 28 July (no lightning due to decaying storm), only the 12–13 July flight was fully successful from the LIS perspective. For direct validation of the spaceborne sensor, the aircraft needed to be flying wings level over an active thunderstorm seen by LIS, whose view time at a specific location is only ~90 s. This is also roughly the expected timing error for experienced ER-2 pilots—responding to instructions from mission scientists in a rapidly changing meteorological environment—to reach a given location at a specific time (e.g., McMurdie et al. 2022). Hence, while underflying the continuously staring GLMs was the default of any ALOFT flight, underflying ISS LIS was an inherently difficult task that was generally only attempted if it did not conflict with, e.g., hunting for gamma rays. The 12–13 July flight was the only flight out of 10 ALOFT flights (Fig. 1) to not detect any glows or TGFs (Table 1), but the fact that direct optical-to-optical validation of LIS with FEGS was achieved does offset that drawback.

Figure 3 summarizes recent validation efforts done with this case. The storm in question was a decaying pulse thunderstorm that developed around sunset in central Florida. ISS LIS was in view of this storm during roughly 0057–0058:45 UTC; however, there is approximately ±3-s uncertainty as LIS view time is defined on a 0.5° grid and the ISS ground speed is ~8000 m s^{-1}. According to AMPR (Fig. 3a), the aircraft had passed the precipitation core of the small storm—where ISS LIS detected four flashes, GLM-16 six flashes, and GLM-18 two flashes (one of which was badly geolocated)—but this was not necessarily an impediment to validation using the ALOFT payload.

In Fig. 3b, LIP detected six distinct electric field changes that matched well with the timing of the six detected GLM-16 flashes. The timings of the four detected ISS LIS flashes

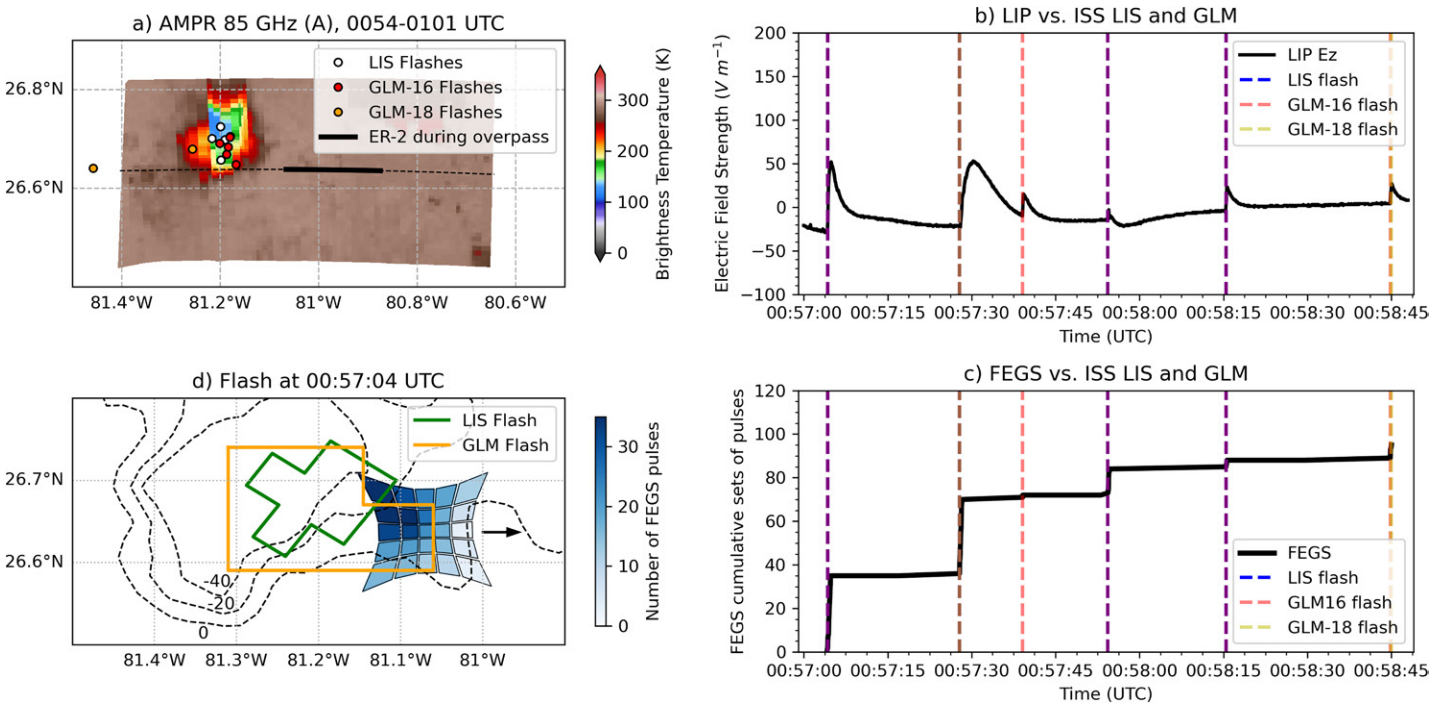

FIG. 3. Overview of the 0054–0101 UTC leg on 13 Jul 2023, near Lake Okeechobee, Florida. Subpanels go clockwise from top left. (a) AMPR 85-GHz (A) channel TBs, as well as the locations of the aircraft (moving eastward) and ISS LIS and GLM-16/GLM-18 flashes during the ISS overpass. (b) Time series of LIP vertical electric field along with the times of LIS and GLM flashes during the overpass, using overlapping colors. In addition to the legend, purple means both LIS and GLM-16 detected, dark brown LIS and GLM-16/GLM-18 detected, and light brown only the two GLMs. (c) As in (b), but showing cumulative 780-nm FEGS pulses. (d) Plan view of the first overpass flash, with *GOES-16* ABI channel 13 brightness temperatures at 0051 UTC (contours; °C), approximate LIS and GLM-16 footprints, and the FEGS field of view with the numbers of pulses observed in each FEGS 780-nm channel.

lined up with four of the six GLM-16 and LIP flashes. The electric field changes weakened progressively toward the end of the viewing period, as the aircraft traveled farther from the storm. FEGS optical pulses agreed with LIP in terms of timing and number of flashes (Fig. 3c), and together the two instruments provided some guidance on why ISS LIS missed the third flash. This appeared to have been an optically and electrically weak flash (e.g., it was the weakest GLM-16 flash of the set, only 27 fJ, and FEGS only detected one pulse group across its array) that occurred about 12 s after the much stronger second flash, and GLM-18 also missed it. The last flash, which occurred around 0058:45 UTC, may not have been in the ISS LIS field of view due to the aforementioned view time uncertainty. But even counting the last flash, LIS detection efficiency (DE) was at worst ~66% for this case, consistent with its previously assessed performance (Blakeslee et al. 2020; Virts et al. 2024).

For spatial comparison, Fig. 3d shows the approximate flash footprints of GLM-16, ISS LIS, and FEGS for the first flash, when the aircraft was closest to the storm. *GOES-16* longwave IR showed midlevel cloud well east of the core, which likely assisted with FEGS detections despite the aircraft's position (Fig. 3a). Unsurprisingly, the Northwest quadrant of the FEGS field of view was the most responsive to this flash, which was behind and to the left of the ER-2. Note the finer spatial resolution of LIS relative to GLM, yet GLM-16 appeared to have better sensitivity to the eastern extent of the optical emissions. FEGS is undergoing a full calibration, which will enable more detailed radiance comparisons for this case (and others).

For all cases, both GLM-16 and GLM-18 flash detection efficiencies were evaluated against FEGS (Table 3). To calculate this, a minimum of 10 pulses needed to be detected by FEGS during straight-and-level flight on station for a flash DE comparison to be triggered. In addition, for a GLM match to occur, an event in the GLM flash needed to be detected within 1 s of the FEGS flash and within 20 km of the aircraft at the time of the flash. Note that the ALOFT

domain is closer to the GLM-16's boresight than GLM-18's (see Fig. 1 of Rudlosky and Virts 2021; GLM-18 coverage is similar to GLM-17), especially in far eastern regions like Florida, so higher DE is expected for GLM-16. The results in Table 3 bore this out, except for the 25 July case. In general, the daytime cases featured worse DE than the nighttime cases, and the more western cases like 6, 24, and 25 July (cf. Fig. 1 vs Table 3) featured the most similar performance between GLM-16 and GLM-18. Meanwhile, GLM-18's DE performance in eastern regions like Florida and San Andres was typically worse than 30%. All of these results matched general expectations.

Interestingly, the best overall performance (especially for GLM-16) was seen for the large mesoscale convective system (MCS) sampled on 24 July (see Marisaldi et al. 2024 for detailed analysis of this case). This nighttime case featured GLM DE as high as 82%, despite also having the highest ratio of 340-nm pulses. Compared to the worst-performing case (28 July, GLM-16 DE 33%), 24 July featured larger mean flash areas (860 vs 539 km^2) and more groups per flash (29 vs 17). 24 July also featured higher average pulses per FEGS flash (12 vs 6). This suggests that GLM performance may suffer greatly in storms with small flashes, particularly when they occur during daytime (like 28 July), in agreement with Zhang and Cummins (2020). However, unlike previous studies that focused on small flashes in intense convection (e.g., Murphy and Said 2020), the 28 July case indicates that this problem also can be significant in weaker storms.

d. Microwave and lightning observations of convection featuring the 29 July 2023 case. The 10th and last science flight for ALOFT occurred on 29 July, and it targeted multicellular sea-breeze thunderstorms over Kennedy Space Center (KSC). This area was well covered by the CFLMA, the KSC interferometer, and a nearby LF sensor (Fig. 1). KSC also has an extensive surface-based field meter network (Lucas et al. 2017). Thus, it is a great example to demonstrate airborne/ground synergies in the ALOFT dataset.

The leg that will be highlighted occurred 2037–2042 UTC (Fig. 4). During this leg, UIB-BGO detected three TGFs (two of which were separated by only 26 ms), though the less-sensitive iSTORM did not detect any. Note that multiple TGFs from the same storm system have been observed before, both from orbit (e.g., Ursi et al. 2016) and during ALOFT (Bjørge-Engeland et al. 2024; Østgaard et al. 2024). Multiple glows were also detected by UIB-BGO (Table 3). As mentioned earlier, all ALOFT flights occurred within the GLM-16/GLM-18 stereo viewing region. However, eastern Florida provides a difficult test for the Mach and Virts (2021) algorithm since it is at the eastern extremity of the GOES-West GLM field of view (Rudlosky and Virts 2021), and as seen in Fig. 3 and Table 3, GLM-18 does not have optimal DE or geolocation there. The CFLMA also measures flash altitudes, while EXRAD and CRS provide crucial cloud-top validation data. At this time, the CFLMA only featured six stations as it was still being installed, so the solutions shown in Fig. 4 were allowed to use a minimum of five stations, increasing DE at the expense of greater location uncertainty.

Of the 50 possible GLM-16 groups that occurred within 10 km of this flight leg, the stereo algorithm was only able to vertically locate 23 with the addition of GLM-18 (Figs. 4a,b). Due to the coarse (~10 km) resolution of the GLM instruments, stereo solutions were noisy, and some were above the EXRAD and CRS echo tops but should not be interpreted as above-cloud lightning. However, on average, the GLM altitudes were above the CFLMA source altitudes (Fig. 4c), which is expected since the stereo algorithm is making use of cloud-top optical signals, while the VHF-based CFLMA can directly map channels inside the cloud. Hand analysis (e.g., Rison et al. 1999) revealed that most of the CFLMA sources between 10 and 15 km MSL were associated with positive charge, with midlevel negative charge below 10 km. This implies the lightning observed by CFLMA was primarily normal polarity. In comparison to EXRAD (Fig. 4d) and CRS (Fig. 4e) vertical structures, near the strongest cell (~27-km along

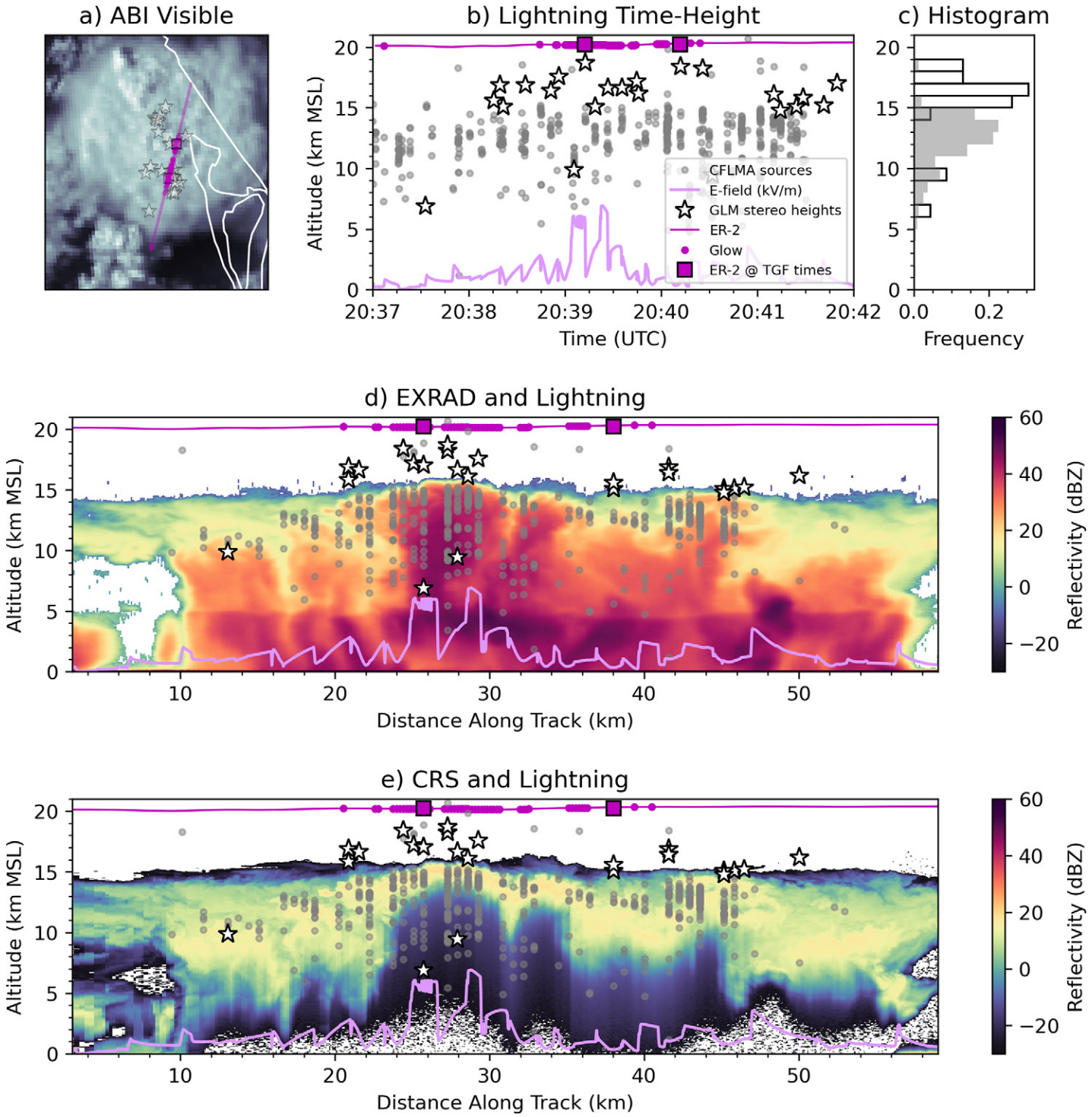

FIG. 4. Overview of the 2037–2042 UTC leg on 29 Jul 2023, near KSC. (a) *GOES-16* ABI visible channel at 2036 UTC, with aircraft track; locations of glows and TGFs; and stereo-analyzed GLM groups [see legend in subplot (b)]. (b) Time–height display of the aircraft, TGFs, glows, electric field magnitude (kV m^{-1}), and stereo GLM group heights, along with CFLMA source locations. (c) Vertical histogram of GLM stereo group and CFLMA source altitudes. (d) Distance–height plot of EXRAD reflectivity along with aircraft, TGF/glow, stereo GLM groups, electric field, and CFLMA sources. (e) As in (d), but for CRS. In all subplots, only lightning within 10 km of the aircraft track is shown.

track), the largest overestimates in stereo heights were seen. Contributing to this error could be the more dynamic cumuliform cloud structure that would be expected in this region. In addition, the aircraft was not fully centered on the main cell during the overflight.

CFLMA showed extensive lightning reaching up to the high-gradient reflectivity region just below the echo top (Figs. 4d,e). The most glows and one TGF occurred near the strongest

turret, and LIP electric field magnitude achieved two separate maxima here (~5–7 kV m^{-1}). This turret featured very strong attenuation at W band (Fig. 4e), especially relative to X band (Fig. 4d). This likely indicated the presence of substantial supercooled liquid water in this turret (e.g., Liao et al. 2008), which could facilitate charge separation, consistent with the presence of strong electric fields and gamma-ray glows. The vertical enhancement in X-band radar reflectivity also is consistent with the radar-based analyses of glowing storms reported by Wada et al. (2021a) and Williams et al. (2022, 2023), confirming those studies' implications that graupel development in thunderclouds enhances electric fields and thereby increases the probability of gamma-ray glows. The second set of glows and the twin TGFs were observed near a different core (~38-km along track), which based on horizontal lightning locations may have been sampled even less directly than the first core (Fig. 4a). Overall, despite the limitations of GLM-18 in this region, there is still useful information content in the GLM cloud altitudes, particularly the clustering of the cloud tops above the CFLMA vertical distribution. Additional analysis of this case, including detailed examination of the interferometer and LF during the TGFs, is ongoing.

The performance of the GLM stereo algorithm across all ALOFT cases is summarized in Table 3. The comparison was against CRS-inferred cloud-top height (CTH; specifically, the height of the −30-dBZ echo top) during straight-and-level flight while on station. Note that during ALOFT, CRS was run in a mode that prevented valid reflectivity observations within 3.5 km of the aircraft. If CTH was observed to be closer than 3.5 km, the CTH was capped to be 3.5 km from the aircraft. Since the ER-2 normally flew within 20–21 km MSL, this CTH cap was variable but typically ranged 16.5–17.5 km. This cap normally did not need to be used except for briefly on a few legs during 24 July; hence, that case's CRS CTH might be biased slightly low. Nonetheless, 24 July had the tallest median CTH (16.6 km), nearly 1 km taller than any other case. Recall that 24 July also had the most detected glows and TGFs (Table 3). An open question is whether the reduced distance between cloud top and the aircraft on 24 July contributed to the increased number of gamma-ray detections relative to other cases since the mean free path of gamma rays can be short (e.g., Williams et al. 2022, 2023).

For GLM stereo height comparisons, both root-mean-square error (RMSE) and bias were computed against CRS. The ABI Enterprise Algorithm Working Group Cloud Height Algorithm (ACHA; Heidinger et al. 2018) also was examined and is reported in Table 3 as well. In general, GLM stereo performance was the worst on low-flash-rate days like 3 and 12 July. However, on certain case days with ample lightning (e.g., 6 July), its performance could exceed the ABI ACHA product as well as the results reported in Mach and Virts (2021). Based on sensitivity analysis (not shown), ACHA RMSE (though not bias) could be substantially improved by excluding cloud-edge regions where CRS's finer resolution led to larger differences between CRS and ACHA CTH. Thus, Table 3 should not be interpreted as a rigorous assessment of ACHA performance, but rather as providing context for interpreting the GLM stereo height results.

e. Microwave and lightning analysis of glowing thunderstorms during ALOFT. As mentioned in section 3a, when hunting for gamma rays, ALOFT mission scientists eventually developed an intuitive feel for targeting the strongest convection in its intensifying to mature stages. While the complexities of using an aircraft to sample rapidly evolving convection made it difficult to always be successful in that endeavor, subsequent analysis has demonstrated that the qualitative perception of the ALOFT team was borne out by the actual data. The results also demonstrated the synergies of combined microwave, lightning, and gamma-ray observations when studying high-energy radiation from thunderstorms.

Figure 5 shows histograms of various ALOFT microwave and lightning observations when glows were detected during on-station, straight-and-level flight. Minimum brightness

temperatures (TBs) in AMPR's 37-GHz (Fig. 5a) and 85-GHz (Fig. 5b) frequencies were extremely low, averaging around 150 and 80 K, respectively, regardless of whether the glowing storm was over land or ocean. These brightness temperatures are indicative of the presence of large ice (e.g., graupel, hail) and are comparable to TBs in severe midlatitude continental hailstorms previously observed by AMPR (Leppert and Cecil 2015; Battaglia et al. 2016), making them among the lowest TBs ever observed by AMPR in its >30-yr history of flight. CoSSIR (Fig. 5c) also observed extremely low TBs across multiple channels when gamma rays were being produced. The median (not peak) EXRAD reflectivity in the column was

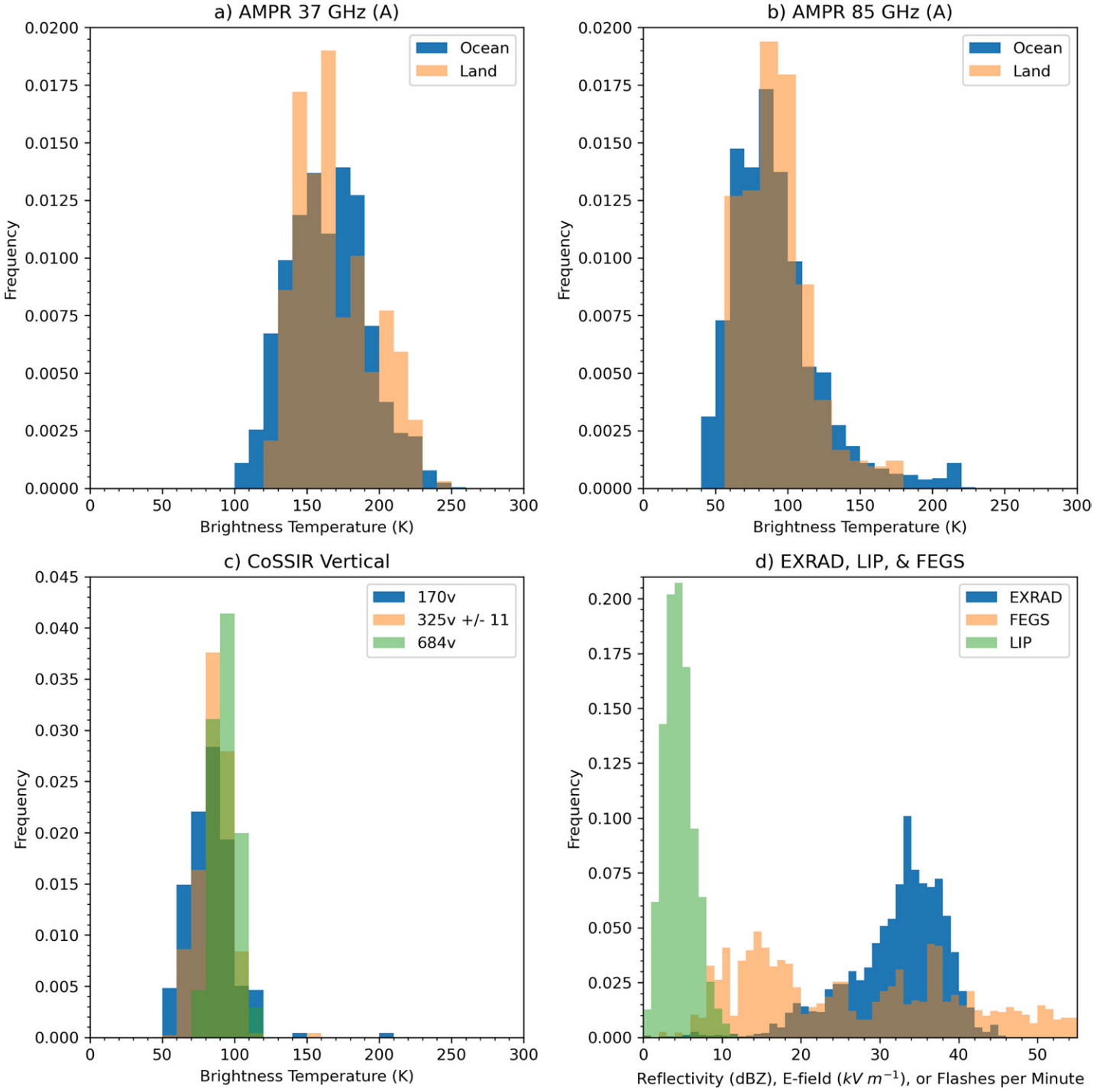

Fig. 5. Histograms of various microwave and lightning observations when glows were detected during all 10 ALOFT flights. (a) Minimum AMPR TBs in the 37-GHz (A) channel, broken out by land vs ocean scenes. (b) As in (a), but for the 85-GHz (A) channel. (c) Minimum CoSSIR TBs in the 170-, 325 ± 11-, and 684-GHz vertical channels (along-track scans only). (d) Histograms of median reflectivities in the EXRAD column, LIP electric field magnitude, and FEGS flash rates.

around 35 dBZ when glows were observed, and even with its limited field of view, FEGS flash rates were almost always at least 6–10 min^{-1} and could reach up to 55 min^{-1} in glowing storms (Fig. 5d). Similar to the snapshot shown in Fig. 4, the statistical analysis of ALOFT radar observations supports the results of Wada et al. (2021a) and Williams et al. (2022, 2023). LIP electric field magnitude during glows averaged ~5 kV m^{-1}, higher than previous combined electric field and glow observations by Østgaard et al. (2019a), as well as higher than the average thunderstorm fields measured by Mach et al. (2009).

Overall, the evidence in Fig. 5, along with the findings of Marisaldi et al. (2024), strongly suggests that (from the perspective of an aircraft flying at 20 km MSL) glows are a phenomenon related to convective intensity, at least in the tropical and subtropical convection sampled by ALOFT. Though not shown here, all distributions in Fig. 5 weakened considerably when UIB-BGO photon counts were indicative of background radiation levels (i.e., <25% enhancement over background). This included nonglowing clouds as well as clear scenes.

4. Summary and conclusions

The ALOFT campaign took significant scientific risks. Going into the field, the team was not certain it would achieve even the minimum objectives of detecting a single glow and a single TGF. However, with extensive preparation, an enthusiastic and well-trained ER-2 crew, and a robust payload that observed many different aspects of convection and lightning, the campaign was able to exploit the (previously unknown) near-ubiquity of gamma-ray production by moderate to intense tropical and subtropical thunderstorms, and thus obtained a unique dataset that should garner cross-cutting interest from the broader meteorological community.

In particular, ALOFT is demonstrating how gamma-ray production likely is a fundamental mode in the evolution of many tropical and subtropical thunderstorms. Far from being a rare phenomenon that may only be of interest to high-energy atmospheric physicists, gamma-ray production likely is common when these thunderstorms are in their intensifying to mature stages, and TGFs are far more common than satellite climatologies suggest (e.g., Bjørge-Engeland et al. 2024). This means gamma-ray production can be an indicator of intense convection, akin to strong electric fields and high lightning flash rates, thus providing useful meteorological information about thunderstorm structure and evolution (or vice versa). This also may have implications for assessments of aviation risk from TGFs (Dwyer et al. 2010; Pallu et al. 2021, 2023).

What remains poorly understood, however, is why satellite-detected TGFs are often limited to the coastal tropics and subtropics (e.g., Fig. 1 inset). One hypothesis may be that, at least in the Americas, coastal regions are well-known foci for organized, deep multicellular thunderstorms, the kind that would be most likely to produce gamma rays as individual cells develop and intensify (Marisaldi et al. 2024). Notably, during ALOFT, the most TGFs and glows were observed in intense mesoscale storms over Campeche Bay on 6 and 24 July (Table 3; see also Marisaldi et al. 2024; Østgaard et al. 2024). In addition, the taller convection in the tropics could provide a greater depth over which to accelerate electrons in strong electric fields, thus making it more likely to develop the RREA needed for gamma-ray production (Dwyer et al. 2012; Fabró et al. 2015), although increased atmospheric absorption of gamma rays in the midlatitudes may also be important (Williams et al. 2006; Smith et al. 2010; Maiorana et al. 2021). Atmospheric absorption may limit the applicability of ALOFT observations for making robust conclusions regarding shallower convection, which also has been shown to produce gamma rays (Williams et al. 2022, 2023). More comprehensive sampling of a wide variety of convection, from aircraft flying at a variety of altitudes, is likely required to fully understand the global phenomenology of glows and TGFs.

Beyond gamma rays, ALOFT provides a rich dataset to assist with the validation of existing spaceborne lightning sensors, as well as informing the development of future

lightning-observing missions. While ISS LIS and GLM detection performance during ALOFT met general expectations, ALOFT found that performance can suffer in weaker storms if flashes are small, so spaceborne optical sensors' detection limits are not just stressed in intense convection. Meanwhile, UV emission from lightning streamers was readily detectable even during daytime and showed variability based on thunderstorm phenomenology, indicating that coupled 337-/777-nm observations have scientific value for the study of thunderstorms and lightning. The performance of stereo heights from the GLM sensors was reasonable relative to 3D lightning mapping observations, as well as comparable to ABI-based products in certain cases, particularly if flash rates were high. This bodes well for the future of the stereo technique given its accuracy is limited by the coarse spatial resolution of the current GLMs (Mach and Virts 2021), which could improve in future sensors. Finally, ALOFT's rapid sampling with a diverse array of active and passive multifrequency sensors enables a process-driven look at thunderstorm evolution, which will benefit the next generation of convection-monitoring satellite missions. In particular, these observations documented the intensity of thunderstorms producing glows, providing important insights into how thunderstorm structure and evolution relates to electrification and high-energy processes.

Acknowledgments. The total number of people involved in some way with ALOFT, across all institutions, easily exceeds 150. In particular, ALOFT would not have been possible without the hard work, skill, and dedication of the NASA Armstrong Flight Research Center (AFRC) ER-2 team for the project, led by project manager Franzeska Becker, pilots H. Dean "Gucci" Neeley and Kirt "Skirt" Stallings, and crew chief Alistair Ma. The ALOFT team is deeply indebted to MacDill Air Force Base, which graciously hosted the ER-2 deployment and provided an excellent center for mission operations. We also thank the governments of México, El Salvador, Nicaragua, Colombia, Belize, Guatemala, and Honduras for generously allowing ER-2 overflights. In addition, Bahamas, Turks and Caicos, Haiti, the Dominican Republic, Costa Rica, Panama, the Cayman Islands, and Jamaica helpfully agreed to overflights ahead of time, though these permissions did not get used during the campaign. NOAA's provision of ABI MDS scanning for 7 of 10 ALOFT flights was a major boon to the campaign; Steve Goodman assisted with ALOFT–NOAA interactions. Major contributors to ALOFT instrument preparation and operations include Monte Bateman, Thomas Edwards, Matthew Fritts, Jose Andres Roncancio Guzmán, Douglas Huie, Bendik Husa, Lihua Li, Yunjiao Pu, Jackson Remington, Jesus Alberto Lopez Trujillo, Michele Urbani, Oscar van der Velde, and Shiming Yang. Aaron Duley of NASA Ames Research Center led MTS support, which was crucial for ALOFT flight operations. The NASA SERVIR program and the LaRC satellite overpass tool team made important contributions to ALOFT forecast planning. John J. Kiriazes of University of Central Florida was integral to the installation of the VHF interferometer at KSC for ALOFT. Earle Williams is thanked for his extensive helpful comments on the manuscript. The ALOFT campaign and the UIB-BGO instrument were supported by the European Research Council under the European Union's Seventh Framework Programme (FP7/2007–13)/ERC Grant Agreement 320839 and the Research Council of Norway under contracts 223252/F50 (CoE) and contract 325582. A reimbursable Space Act Agreement enabled these funds to support NASA operations. Drs. Jack Kaye and Will McCarty of NASA Headquarters, as well as the NASA Earth from ISS program, are gratefully acknowledged for the provision of additional supplemental funds for ALOFT instruments and operations. Work on ALOFT at the U.S. Naval Research Laboratory (NRL) was supported by the Office of Naval Research 6.1 funds. In addition, coauthor Shy was supported by NRL's Jerome and Isabella Karle Fellowship. The CoSSIR team acknowledges contributions from the NASA Airborne Instrument Technology Transition program (NNH19ZDA001N-AITT) that operationalized CoSSIR for flight on the ER-2. The Yucatán LF deployment was supported by grant UNAM DGAPA IA105123. The UPC work was supported by research grants from the Spanish Ministry (MCIN/AEI/10.13039/501100011033): PID2019-109269RB-C42, PID2022-136348NB-C32, and EQC2021-00695-P, and from the AGAUR Grant 2020 FI-B 00533. Georgia Tech ground LF receiver contributions were supported by the National

Science Foundation (NSF) under Grants AGS-2221765484 and AGS-2139916. New Mexico Tech involvement in ALOFT was sponsored by NSF Grant AGS-2214044. Support for coauthor Bitzer was provided by NSF Grant DEB-2213247.

Data availability statement. The ALOFT dataset is being hosted publicly by the NASA Global Hydrometeorology Resource Center (GHRC) Distributed Active Archive Center (DAAC) at https://doi.org/10.5067/ALOFT/DATA101. The goes2go software (https://goes2go.readthedocs.io/) was used to automate the download of ABI and GLM data from NOAA online archives. ISS LIS data are available from https://doi.org/10.5067/LIS/ISSLIS/DATA111.

References

Amiot, C. G., S. K. Biswas, T. J. Lang, and D. I. Duncan, 2021: Dual-polarization deconvolution and geophysical retrievals from the advanced microwave precipitation radiometer during OLYMPEX/RADEX. *J. Atmos. Oceanic Technol.*, **38**, 607–628, https://doi.org/10.1175/JTECH-D-19-0218.1.

Atmosphere Observing System, 2024: Atmosphere observing system. https://aos.gsfc.nasa.gov/.

Barnes, D. E., M. E. Splitt, J. R. Dwyer, S. Lazarus, D. M. Smith, and H. K. Rassoul, 2015: A study of thunderstorm microphysical properties and lightning flash counts associated with terrestrial gamma-ray flashes. *J. Geophys. Res. Atmos.*, **120**, 3453–3464, https://doi.org/10.1002/2014JD021495.

Battaglia, A., K. Mroz, T. Lang, F. Tridon, S. Tanelli, L. Tian, and G. M. Heymsfield, 2016: Using a multiwavelength suite of microwave instruments to investigate the microphysical structure of deep convective cores. *J. Geophys. Res. Atmos.*, **121**, 9356–9381, https://doi.org/10.1002/2016JD025269.

Belz, J. W., and Coauthors, 2020: Observations of the origin of downward terrestrial gamma-ray flashes. *J. Geophys. Res. Atmos.*, **125**, e2019JD031940, https://doi.org/10.1029/2019JD031940.

Bjørge-Engeland, I., and Coauthors, 2024: Evidence of a new population of weak terrestrial Gamma-ray Flashes observed from aircraft altitude. *Geophys. Res. Lett.*, **51**, e2024GL110395, https://doi.org/10.1029/2024GL110395.

Blakeslee, R. J., and Coauthors, 2020: Three years of the Lightning Imaging Sensor onboard the International Space Station: Expanded global coverage and enhanced applications. *J. Geophys. Res. Atmos.*, **125**, e2020JD032918, https://doi.org/10.1029/2020JD032918.

Bowers, G. S., and Coauthors, 2018: A terrestrial gamma-ray flash inside the eyewall of Hurricane Patricia. *J. Geophys. Res. Atmos.*, **123**, 4977–4987, https://doi.org/10.1029/2017JD027771.

Briggs, M. S., and Coauthors, 2013: Terrestrial gamma-ray flashes in the Fermi era: Improved observations and analysis methods. *J. Geophys. Res. Space Phys.*, **118**, 3805–3830, https://doi.org/10.1002/jgra.50205.

Chilingarian, A., G. Hovsepyan, and A. Hovhannisyan, 2011: Particle bursts from thunderclouds: Natural particle accelerators above our heads. *Phys. Rev.*, **83D**, 062001, https://doi.org/10.1103/PhysRevD.83.062001.

Chronis, T., and Coauthors, 2016: Characteristics of thunderstorms that produce terrestrial gamma ray flashes. *Bull. Amer. Meteor. Soc.*, **97**, 639–653, https://doi.org/10.1175/BAMS-D-14-00239.1.

Cohen, M., R. Said, E. Paschal, J. McCormick, N. Gross, L. Thompson, U. Inan, and J. C. Chang, 2018: Broadband longwave remote sensing instrumentation. *Rev. Sci. Instrum.*, **89**, 094501, https://doi.org/10.1063/1.5041419.

Cummer, S. A., Y. Zhai, W. Hu, D. M. Smith, L. I. Lopez, and M. A. Stanley, 2005: Measurements and implications of the relationship between lightning and terrestrial gamma ray flashes. *Geophys. Res. Lett.*, **32**, L08811, https://doi.org/10.1029/2005GL022778.

——, G. Lu, M. S. Briggs, V. Connaughton, S. Xiong, G. J. Fishman, and J. R. Dwyer, 2011: The lightning-TGF relationship on microsecond timescales. *Geophys. Res. Lett.*, **38**, L14810, https://doi.org/10.1029/2011GL048099.

——, and Coauthors, 2014: The source altitude, electric current, and intrinsic brightness of terrestrial gamma ray flashes. *Geophys. Res. Lett.*, **41**, 8586–8593, https://doi.org/10.1002/2014GL062196.

Curtis, S., 2004: Diurnal cycle of rainfall and surface winds and the mid-summer drought of Mexico/Central America. *Climate Res.*, **27** (1), 1–8, https://doi.org/10.3354/cr027001.

da Silva, C. L., and V. P. Pasko, 2013: Dynamics of streamer-to-leader transition at reduced air densities and its implications for propagation of lightning leaders and gigantic jets. *J. Geophys. Res. Atmos.*, **118**, 13 561–13 590, https://doi.org/10.1002/2013JD020618.

Dolan, B., and Coauthors, 2023: Time resolved reflectivity measurements of convective clouds. *Geophys. Res. Lett.*, **50**, e2023GL105723, https://doi.org/10.1029/2023GL105723.

Dwyer, J. R., 2012: The relativistic feedback discharge model of terrestrial gamma ray flashes. *J. Geophys. Res.*, **117**, A02308, https://doi.org/10.1029/2011JA017160.

——, and D. M. Smith, 2005: A comparison between Monte Carlo simulations of runaway breakdown and terrestrial gamma-ray flash observations. *Geophys. Res. Lett.*, **32**, L22804, https://doi.org/10.1029/2005GL023848.

——, ——, M. A. Uman, Z. Saleh, B. Grefenstette, B. Hazelton, and H. K. Rassoul, 2010: Estimation of the fluence of high-energy electron bursts produced by thunderclouds and the resulting radiation doses received in aircraft. *J. Geophys. Res.*, **115**, D09206, https://doi.org/10.1029/2009JD012039.

——, ——, and S. A. Cummer, 2012: High-energy atmospheric physics: Terrestrial gamma-ray flashes and related phenomena. *Space Sci. Rev.*, **173**, 133–196, https://doi.org/10.1007/s11214-012-9894-0.

Eack, K. B., and W. H. Beasley, 2015: Long-duration X-ray emissions observed in thunderstorms. *J. Geophys. Res. Atmos.*, **120**, 6887–6897, https://doi.org/10.1002/2015JD023262.

Fabró, F., J. Montanyà, M. Marisaldi, O. A. van der Velde, and F. Fuschino, 2015: Analysis of global Terrestrial Gamma Ray Flashes distribution and special focus on AGILE detections over South America. *J. Atmos. Sol.-Terr. Phys.*, **124**, 10–20, https://doi.org/10.1016/j.jastp.2015.01.009.

Fishman, G. J., and Coauthors, 1994: Discovery of intense gamma-ray flashes of atmospheric origin. *Science*, **264**, 1313–1316, https://doi.org/10.1126/science.264.5163.1313.

Fuschino, F., and Coauthors, 2011: High spatial resolution correlation of AGILE TGFs and global lightning activity above the equatorial belt. *Geophys. Res. Lett.*, **38**, L14806, https://doi.org/10.1029/2011GL047817.

Grefenstette, B. W., D. M. Smith, B. J. Hazelton, and L. I. Lopez, 2009: First RHESSI terrestrial gamma ray flash catalog. *J. Geophys. Res.*, **114**, A02314, https://doi.org/10.1029/2008JA013721.

Halverson, J., and Coauthors, 2007: NASA's Tropical Cloud Systems and Processes experiment. *Bull. Amer. Meteor. Soc.*, **88**, 867–882, https://doi.org/10.1175/BAMS-88-6-867.

Heidinger, A. K., Y. Li, and S. Wanzong, 2018: Enterprise AWG Cloud Height Algorithm (ACHA). NOAA NESDIS Center for Satellite Applications and Research, 72 pp., https://www.star.nesdis.noaa.gov/jpss/documents/ATBD/ATBD_EPS_Cloud_ACHA_v3.4.pdf.

Heumesser, M., and Coauthors, 2021: Spectral observations of optical emissions associated with Terrestrial Gamma-Ray Flashes. *Geophys. Res. Lett.*, **48**, e2020GL090700, https://doi.org/10.1029/2020GL090700.

Heymsfield, G. M., L. Li, M. L. Walker McLinden, L. Liao, C. N. Helms, and S. Guimond, 2024: NASA high altitude airborne weather radars. *Advances in Weather Radar: Precipitation Science, Scattering and Processing Algorithms*, V. N. Bringi, K. V. Mishra, and M. Thurai, Eds., Vol. 1, IET, 231–282.

Husbjerg, L. S., and Coauthors, 2022: Observations of blue corona discharges in thunderclouds. *Geophys. Res. Lett.*, **49**, e2022GL099064, https://doi.org/10.1029/2022GL099064.

Jensen, D. P., R. G. Sonnenfeld, M. A. Stanley, H. E. Edens, C. L. da Silva, and P. R. Krehbiel, 2021: Dart-leader and K-leader velocity from initiation site to termination time-resolved with 3D interferometry. *J. Geophys. Res. Atmos.*, **126**, e2020JD034309, https://doi.org/10.1029/2020JD034309.

Jensen, M. P., and Coauthors, 2016: The Midlatitude Continental Convective Clouds Experiment (MC3E). *Bull. Amer. Meteor. Soc.*, **97**, 1667–1686, https://doi.org/10.1175/BAMS-D-14-00228.1.

Kelley, N. A., and Coauthors, 2015: Relativistic electron avalanches as a thunderstorm discharge competing with lightning. *Nat. Commun.*, **6**, 7845, https://doi.org/10.1038/ncomms8845.

Kochkin, P., and Coauthors, 2017: In-flight observation of gamma ray glows by ILDAS. *J. Geophys. Res. Atmos.*, **122**, 12 801–12 811, https://doi.org/10.1002/2017JD027405.

——, and Coauthors, 2021: A rapid gamma-ray glow flux reduction observed from 20 km altitude. *J. Geophys. Res. Atmos.*, **126**, e2020JD033467, https://doi.org/10.1029/2020JD033467.

Kroodsma, R., 2024: Compact Scanning Submillimeter-wave Imaging Radiometer (CoSSIR) IMPACTS. NASA Global Hydrometeorology Resource Center DAAC, accessed 14 October 2024, https://doi.org/10.5067/IMPACTS/COSSIR/DATA101.

Kuriyama, E., and Coauthors, 2022: Compton camera imaging of a gamma-ray glow from a thunderstorm. *Geophys. Res. Lett.*, **49**, e2022GL100139, https://doi.org/10.1029/2022GL100139.

Lang, T. J., 2023: Validation of the geostationary lightning mapper with a lightning mapping array in Argentina: Implications for current and future spaceborne lightning observations. *Earth Space Sci.*, **10**, e2023EA002998, https://doi.org/10.1029/2023EA002998.

Larkey, R. K., J. G. Sample, D. M. Smith, J. L. Lapierre, E. DiGangi, and R. H. Holzworth, 2021: The relationship between TGF production in thunderstorms and lightning flash rates and amplitudes. *J. Geophys. Res. Atmos.*, **126**, e2020JD034401, https://doi.org/10.1029/2020JD034401.

Leppert, K. D., and D. J. Cecil, 2015: Signatures of hydrometeor species from airborne passive microwave data for frequencies 10–183 GHz. *J. Appl. Meteor. Climatol.*, **54**, 1313–1334, https://doi.org/10.1175/JAMC-D-14-0145.1.

Liao, L., R. Meneghini, L. Tian, and G. M. Heymsfield, 2008: Retrieval of snow and rain from combined X- and W-band airborne radar measurements. *IEEE Trans. Geosci. Remote Sens.*, **46**, 1514–1524, https://doi.org/10.1109/TGRS.2008.916079.

Lindanger, A., and Coauthors, 2020: The 3rd AGILE terrestrial gamma ray flash catalog. Part I: Association to lightning sferics. *J. Geophys. Res. Atmos.*, **125**, e2019JD031985, https://doi.org/10.1029/2019JD031985.

——, and Coauthors, 2022: Production of terrestrial gamma-ray flashes during the early stages of lightning flashes. *J. Geophys. Res. Atmos.*, **127**, e2021JD036305, https://doi.org/10.1029/2021JD036305.

Liu, C., and E. J. Zipser, 2008: Diurnal cycles of precipitation, clouds, and lightning in the tropics from 9 years of TRMM observations. *Geophys. Res. Lett.*, **35**, L04819, https://doi.org/10.1029/2007GL032437.

Lucas, G. M., J. P. Thayer, and W. Deierling, 2017: Statistical analysis of spatial and temporal variations in atmospheric electric fields from a regional array of field mills. *J. Geophys. Res. Atmos.*, **122**, 1158–1174, https://doi.org/10.1002/2016JD025944.

Lyu, F., S. A. Cummer, M. Briggs, D. M. Smith, B. Mailyan, and S. Lesage, 2021: Terrestrial gamma-ray flashes can be detected with radio measurements of energetic in-cloud pulses during thunderstorms. *Geophys. Res. Lett.*, **48**, e2021GL093627, https://doi.org/10.1029/2021GL093627.

Mach, D., and K. Virts, 2021: A technique for determining three-dimensional storm cloud-top locations using stereo optical lightning pulses observed from orbit. *J. Atmos. Oceanic Technol.*, **38**, 1993–2001, https://doi.org/10.1175/JTECH-D-21-0078.1.

Mach, D. M., R. J. Blakeslee, M. G. Bateman, and J. C. Bailey, 2009: Electric fields, conductivity, and estimated currents from aircraft overflights of electrified clouds. *J. Geophys. Res.*, **114**, D10204, https://doi.org/10.1029/2008JD011495.

Maiorana, C., and Coauthors, 2020: The 3rd AGILE terrestrial gamma-ray flashes catalog. Part II: Optimized selection criteria and characteristics of the new sample. *J. Geophys. Res. Atmos.*, **125**, e2019JD031986, https://doi.org/10.1029/2019JD031986.

——, and Coauthors, 2021: Observation of Terrestrial Gamma-ray Flashes at mid latitude. *J. Geophys. Res. Atmos.*, **126**, e2020JD034432, https://doi.org/10.1029/2020JD034432.

Marchand, M., K. Hilburn, and S. D. Miller, 2019: Geostationary Lightning Mapper and Earth networks lightning detection over the contiguous united states and dependence on flash characteristics. *J. Geophys. Res. Atmos.*, **124**, 11 552–11 567, https://doi.org/10.1029/2019JD031039.

Marisaldi, M., and Coauthors, 2013: Terrestrial gamma-ray flashes. *Nucl. Instrum. Methods Phys.: Res.*, **720A**, 83–87, https://doi.org/10.1016/j.nima.2012.12.029.

——, and Coauthors, 2024: Highly dynamic gamma-ray emissions are common in tropical thunderclouds. *Nature*, **634**, 57–60, https://doi.org/10.1038/s41586-024-07936-6.

McMurdie, L. A., and Coauthors, 2022: Chasing snowstorms: The Investigation of Microphysics and Precipitation for Atlantic Coast-Threatening Snowstorms (IMPACTS) campaign. *Bull. Amer. Meteor. Soc.*, **103**, E1243–E1269, https://doi.org/10.1175/BAMS-D-20-0246.1.

Morales Rodriguez, C. A., J. Montanyà, O. A. van der Velde, F. Fabró, and J. A. Lopez, 2021: Tropical TGF paradox: A perspective from TRMM precipitation radar. *J. Geophys. Res. Atmos.*, **126**, e2021JD034698, https://doi.org/10.1029/2021JD034698.

Murphy, M. J., and R. K. Said, 2020: Comparisons of lightning rates and properties from the U.S. National Lightning Detection Network (NLDN) and GLD360 with GOES-16 Geostationary Lightning Mapper and advanced baseline imager data. *J. Geophys. Res. Atmos.*, **125**, e2019JD031172, https://doi.org/10.1029/2019JD031172.

Neubert, T., and Coauthors, 2019: The ASIM mission on the International Space Station. *Space Sci. Rev.*, **215**, 26, https://doi.org/10.1007/s11214-019-0592-z.

Østgaard, N., and Coauthors, 2019a: Gamma ray glow observations at 20-km altitude. *J. Geophys. Res. Atmos.*, **124**, 7236–7254, https://doi.org/10.1029/2019JD030312.

——, and Coauthors, 2019b: First 10 months of TGF observations by ASIM. *J. Geophys. Res. Atmos.*, **124**, 14 024–14 036, https://doi.org/10.1029/2019JD031214.

——, and Coauthors, 2024: Flickering gamma-ray flashes, the missing link between gamma glows and TGFs. *Nature*, **634**, 53–56, https://doi.org/10.1038/s41586-024-07893-0.

Pallu, M., S. Celestin, F. Trompier, and M. Klerlein, 2021: Estimation of radiation doses delivered by terrestrial gamma ray flashes within leader-based production models. *J. Geophys. Res. Atmos.*, **126**, e2020JD033907, https://doi.org/10.1029/2020JD033907.

——, ——, ——, and ——, 2023: Radiation risk assessment associated with terrestrial gamma ray flashes for commercial flights. *J. Geophys. Res. Atmos.*, **128**, e2022JD037569, https://doi.org/10.1029/2022JD037569.

Parks, G. K., B. H. Mauk, R. Spiger, and J. Chin, 1981: X-ray enhancements detected during thunderstorm and lightning activities. *Geophys. Res. Lett.*, **8**, 1176–1179, https://doi.org/10.1029/GL008i011p01176.

Pu, Y., and S. A. Cummer, 2024: Imaging step formation in In-cloud lightning initial development with VHF interferometry. *Geophys. Res. Lett.*, **51**, e2023GL107388, https://doi.org/10.1029/2023GL107388.

——, ——, F. Lyu, M. Briggs, B. Mailyan, M. Stanbro, and O. Roberts, 2019: Low frequency radio pulses produced by terrestrial gamma-ray flashes. *Geophys. Res. Lett.*, **46**, 6990–6997, https://doi.org/10.1029/2019GL082743.

——, ——, A. Huang, M. Briggs, B. Mailyan, and S. Lesage, 2020: A satellite-detected terrestrial gamma ray flash produced by a cloud-to-ground lightning leader. *Geophys. Res. Lett.*, **47**, e2020GL089427, https://doi.org/10.1029/2020GL089427.

Quick, M. G., H. J. Christian, K. S. Virts, and R. J. Blakeslee, 2020: Airborne radiometric validation of the geostationary lightning mapper using the fly's eye GLM simulator. *J. Appl. Remote Sens.*, **14**, 044518, https://doi.org/10.1117/1.JRS.14.044518.

Reinhart, B., and Coauthors, 2014: Understanding the relationships between lightning, cloud microphysics, and airborne radar-derived storm structure during Hurricane Karl (2010). *Mon. Wea. Rev.*, **142**, 590–605, https://doi.org/10.1175/MWR-D-13-00008.1.

Remington, J. R., P. N. Gatlin, S. M. Stough, N. Pailoor, S. A. Behnke, T. J. Lang, and H. E. Edens, 2024: Simulated feasibility of 3-D lightning mapping from space. *IEEE Trans. Geosci. Remote Sens.*, **62**, 1–9, https://doi.org/10.1109/TGRS.2024.3398508.

Rison, W., R. Thomas, P. Krehbiel, T. Hamlin, and J. Harlin, 1999: A GPS-based three-dimensional lightning mapping system: Initial observations in Central New Mexico. *Geophys. Res. Lett.*, **26**, 3573–3576, https://doi.org/10.1029/1999GL010856.

Rudlosky, S. D., and K. S. Virts, 2021: Dual Geostationary Lightning Mapper observations. *Mon. Wea. Rev.*, **149**, 979–998, https://doi.org/10.1175/MWR-D-20-0242.1.

——, S. J. Goodman, K. S. Virts, and E. C. Bruning, 2019: Initial Geostationary Lightning Mapper observations. *Geophys. Res. Lett.*, **46**, 1097–1104, https://doi.org/10.1029/2018GL081052.

Rutledge, S. A., K. A. Hilburn, A. Clayton, B. Fuchs, and S. D. Miller, 2020: Evaluating Geostationary Lightning Mapper flash rates within intense convective storms. *J. Geophys. Res. Atmos.*, **125**, e2020JD032827, https://doi.org/10.1029/2020JD032827.

Schultz, C. J., and Coauthors, 2021: Remote sensing of electric fields observed within winter precipitation during the 2020 Investigation of Microphysics and Precipitation for Atlantic Coast-Threatening Snowstorms (IMPACTS) field campaign. *J. Geophys. Res. Atmos.*, **126**, e2021JD034704, https://doi.org/10.1029/2021JD034704.

Skeie, C. A., N. Østgaard, A. Mezentsev, I. Bjørge-Engeland, M. Marisaldi, N. Lehtinen, V. Reglero, and T. Neubert, 2022: The temporal relationship between Terrestrial Gamma-ray Flashes and associated optical pulses from lightning. *J. Geophys. Res. Atmos.*, **127**, e2022JD037128, https://doi.org/10.1029/2022JD037128.

Skofronick-Jackson, G., and Coauthors, 2015: Global Precipitation Measurement Cold Season Precipitation Experiment (GCPEX): For measurement's sake, let it snow. *Bull. Amer. Meteor. Soc.*, **96**, 1719–1741, https://doi.org/10.1175/BAMS-D-13-00262.1.

Smith, D. M., B. J. Hazelton, B. W. Grefenstette, J. R. Dwyer, R. H. Holzworth, and E. H. Lay, 2010: Terrestrial gamma ray flashes correlated to storm phase and tropopause height. *J. Geophys. Res.*, **115**, A00E49, https://doi.org/10.1029/2009JA014853.

——, and Coauthors, 2011a: A terrestrial gamma ray flash observed from an aircraft. *J. Geophys. Res.*, **116**, D20124, https://doi.org/10.1029/2011JD016252.

——, and Coauthors, 2011b: The rarity of terrestrial gamma-ray flashes. *Geophys. Res. Lett.*, **38**, L08807, https://doi.org/10.1029/2011GL046875.

Soler, S., and Coauthors, 2020: Blue optical observations of narrow bipolar events by ASIM suggest corona streamer activity in thunderstorms. *J. Geophys. Res. Atmos.*, **125**, e2020JD032708, https://doi.org/10.1029/2020JD032708.

Splitt, M. E., S. M. Lazarus, D. Barnes, J. R. Dwyer, H. K. Rassoul, D. M. Smith, B. Hazelton, and B. Grefenstette, 2010: Thunderstorm characteristics associated with RHESSI identified terrestrial gamma ray flashes. *J. Geophys. Res.*, **115**, A00E38, https://doi.org/10.1029/2009JA014622.

Stanley, M. A., X.-M. Shao, D. M. Smith, L. I. Lopez, M. B. Pongratz, J. D. Harlin, M. Stock, and A. Regan, 2006: A link between terrestrial gamma-ray flashes and intracloud lightning discharges. *Geophys. Res. Lett.*, **33**, L06803, https://doi.org/10.1029/2005GL025537.

Tiberia, A., and Coauthors, 2021: GPM-DPR observations on TGFs producing storms. *J. Geophys. Res. Atmos.*, **126**, e2020JD033647, https://doi.org/10.1029/2020JD033647.

Tierney, D., and Coauthors, 2013: Fluence distribution of terrestrial gamma ray flashes observed by the Fermi Gamma-ray Burst Monitor. *J. Geophys. Res. Space Phys.*, **118**, 6644–6650, https://doi.org/10.1002/jgra.50580.

Tran, M. D., V. A. Rakov, S. Mallick, J. R. Dwyer, A. Nag, and S. Heckman, 2015: A terrestrial gamma-ray flash recorded at the Lightning Observatory in Gainesville, Florida. *J. Atmos. Sol.-Terr. Phys.*, **136**, 86–93, https://doi.org/10.1016/j.jastp.2015.10.010.

Urbani, M., J. Montanyà, O. A. van der Velde, J. A. López, M. Arcanjo, P. Fontanes, D. Romero, and J. A. Roncancio, 2021: High-energy radiation from natural lightning observed in coincidence with a VHF broadband interferometer. *J. Geophys. Res. Atmos.*, **126**, e2020JD033745, https://doi.org/10.1029/2020JD033745.

Ursi, A., M. Marisaldi, M. Tavani, D. Casella, P. Sanò, and S. Dietrich, 2016: Detection of multiple terrestrial gamma-ray flashes from thunderstorm systems. *J. Geophys. Res. Space Phys.*, **121**, 11 302–11 315, https://doi.org/10.1002/2016JA023136.

——, ——, S. Dietrich, M. Tavani, A. Tiberia, and F. Porcu, 2019: Analysis of thunderstorms producing Terrestrial Gamma Ray Flashes with the Meteosat Second Generation. *J. Geophys. Res. Atmos.*, **124**, 12 667–12 682, https://doi.org/10.1029/2018JD030149.

van der Velde, O. A., and Coauthors, 2024: Imaging of 3 bright terrestrial gamma-ray flashes by the atmosphere-space interactions monitor and their parent thunderstorms. *Sci. Rep.*, **14**, 6946, https://doi.org/10.1038/s41598-024-57229-1.

Virts, K. S., T. J. Lang, D. E. Buechler, and P. M. Bitzer, 2024: Bayesian analysis of the detection performance of the Lightning Imaging Sensors. *J. Atmos. Oceanic Technol.*, **41**, 441–455, https://doi.org/10.1175/JTECH-D-23-0090.1.

Wada, Y., and Coauthors, 2019a: Gamma-ray glow preceding downward terrestrial gamma-ray flash. *Commun. Phys.*, **2**, 67, https://doi.org/10.1038/s42005-019-0168-y.

——, and Coauthors, 2019b: Downward terrestrial gamma-ray flash observed in a winter thunderstorm. *Phys. Rev. Lett.*, **123**, 061103, https://doi.org/10.1103/PhysRevLett.123.061103.

——, and Coauthors, 2020: High peak-current lightning discharges associated with downward terrestrial gamma-ray flashes. *J. Geophys. Res. Atmos.*, **125**, e2019JD031730, https://doi.org/10.1029/2019JD031730.

——, and Coauthors, 2021a: Meteorological aspects of gamma-ray glows in winter thunderstorms. *Geophys. Res. Lett.*, **48**, e2020GL091910, https://doi.org/10.1029/2020GL091910.

——, and Coauthors, 2021b: Catalog of gamma-ray glows during four winter seasons in Japan. *Phys. Rev. Res.*, **3**, 043117, https://doi.org/10.1103/PhysRevResearch.3.043117.

——, and Coauthors, 2023: Termination of downward-oriented gamma-ray glow by normal-polarity in-cloud discharge activity. *J. Geophys. Res. Atmos.*, **128**, e2023JD038606, https://doi.org/10.1029/2023JD038606.

Walker, T. D., and H. J. Christian, 2017: Triggered lightning spectroscopy: Part 1. A qualitative analysis. *J. Geophys. Res. Atmos.*, **122**, 8000–8011, https://doi.org/10.1002/2016JD026419.

Walker McLinden, M. L., L. Li, G. M. Heymsfield, M. Coon, and A. Emory, 2021: The NASA GSFC 94-GHz airborne solid-state Cloud Radar System (CRS). *J. Atmos. Oceanic Technol.*, **38**, 1001–1017, https://doi.org/10.1175/JTECH-D-20-0127.1.

Williams, E., and Coauthors, 2006: Lightning flashes conducive to the production and escape of gamma radiation to space. *J. Geophys. Res.*, **111**, D16209, https://doi.org/10.1029/2005JD006447.

——, H. Mkrtchyan, B. Mailyan, G. Karapetyan, and S. Hovakimyan, 2022: Radar diagnosis of the thundercloud electron accelerator. *J. Geophys. Res. Atmos.*, **127**, e2021JD035957, https://doi.org/10.1029/2021JD035957.

——, B. Mailyan, G. Karapetyan, and H. Mkrtchyan, 2023: Conditions for energetic electrons and gamma rays in thunderstorm ground enhancements. *J. Geophys. Res. Atmos.*, **128**, e2023JD039612, https://doi.org/10.1029/2023JD039612.

Yanoviak, S. P., E. M. Gora, J. M. Burchfield, P. M. Bitzer, and M. Detto, 2017: Quantification and identification of lightning damage in tropical forests. *Ecol. Evol.*, **7**, 5111–5122, https://doi.org/10.1002/ece3.3095.

Zhang, D., and K. L. Cummins, 2020: Time evolution of satellite-based optical properties in lightning flashes, and its impact on GLM flash detection. *J. Geophys. Res. Atmos.*, **125**, e2019JD032024, https://doi.org/10.1029/2019JD032024.

Zhu, Y., and Coauthors, 2020: Huntsville Alabama Marx Meter Array 2: Upgrade and capability. *Earth Space Sci.*, **7**, e2020EA001111, https://doi.org/10.1029/2020EA001111.